



OPEN

SUBJECT AREAS:  
MATERIALS SCIENCE  
MATERIALS FOR DEVICESReceived  
17 October 2013Accepted  
28 March 2014Published  
15 April 2014Correspondence and  
requests for materials  
should be addressed to  
Z.A.T. (tanzhanao@  
ncepu.edu.cn) or Y.F.L.  
(liyf@iccas.ac.cn)

# High performance polymer solar cells with as-prepared zirconium acetylacetonate film as cathode buffer layer

Zhan'ao Tan<sup>1</sup>, Shusheng Li<sup>1</sup>, Fuzhi Wang<sup>1</sup>, Deping Qian<sup>1</sup>, Jun Lin<sup>1</sup>, Jianhui Hou<sup>2</sup> & Yongfang Li<sup>2</sup>

<sup>1</sup>State Key Laboratory of Alternate Electrical Power System with Renewable Energy Sources, Beijing Key Laboratory of Energy Security and Clean Utilization, North China Electric Power University, Beijing 102206, China, <sup>2</sup>Beijing National Laboratory for Molecular Sciences, Institute of Chemistry, Chinese Academy of Sciences, Beijing 100190, China.

Low-work-function active metals are commonly used as cathode in polymer solar cells (PSCs), but sensitivity of the active metals towards moisture and oxygen results in poor stability of the devices. Therefore, solution-processable and stable cathode buffer layer is of great importance for the application of PSCs. Here we demonstrate high performance PSCs by employing as-prepared zirconium acetylacetonate (a-ZrAcac) film spin-cast from its ethanol solution as cathode buffer layer. The PSCs based on a low bandgap polymer PBDTBDD as donor and PC<sub>60</sub>BM as acceptor with a-ZrAcac/Al cathode demonstrated an average power conversion efficiency (PCE) of 8.75% which is significantly improved than that of the devices with traditional Ca/Al cathode. The improved photovoltaic performance is benefitted from the decreased series resistance and enhanced light harvest of the PSCs with the a-ZrAcac/Al cathode. The results indicate that a-ZrAcac is a promising high performance cathode buffer layer for fabricating large area flexible PSCs.

Since the first reports of photo-induced electron transfer from a conjugated polymer to fullerene<sup>1</sup>, polymer solar cells (PSCs) have attracted exclusive attention due to low-cost, light-weight, and mechanical flexibility with compatibility to future large-area roll-to-roll printing production. The performance of PSCs depends not only on the electronic energy levels, absorption and carrier mobility of the conjugated polymer donor and fullerene derivative acceptor photovoltaic materials<sup>2–5</sup>, but also on the effective charge extraction of both holes and electrons from the photoactive layer and then collection to the respective anode and cathode<sup>6–9</sup>. Therefore, the electrode materials or the electrode buffer layers play a key role in improving photovoltaic performance of the PSCs<sup>7,8</sup>. High workfunction anode buffer layers and low workfunction cathode buffer layers are pursued in selecting the electrode buffer layers.

Low-work-function active metals, such as Ca, Ba and Mg, are commonly used as cathode for efficient electron extraction in PSCs, but the active metals are very sensitive to environmental moisture and oxygen, resulting in poor stability of the devices<sup>10–14</sup>. Therefore, solution-processable and stable cathode buffer layer (CBL) is of great importance for promoting the application of PSCs<sup>15–17</sup>. Recently, solution processable transition metal oxides (ZnO<sup>18–21</sup> and TiOx<sup>22–25</sup>), transition metal chelates<sup>26–30</sup>, and conjugated polyelectrolytes<sup>31–33</sup>, have been successfully used as the CBLs. Nevertheless, compared with anode buffer layer, the CBL is still very limited, and air-stable, facile-processed, easily obtained CBLs are in great request. Recently, a wide bandgap oxide, zirconium oxide (ZrO<sub>2</sub>), deposited by spray pyrolysis<sup>34</sup>, electron beam evaporation<sup>35</sup> or atomic layer deposition<sup>36</sup>, was successfully utilized as electron injection layer in inverse and conventional polymer light-emitting diodes. The greatly enhancement in device performance was attributed to the suitable energy levels of ZrO<sub>2</sub> which have hole-blocking and electron injection ability<sup>34–36</sup>. However, there is no report about using zirconium based materials as CBLs in PSCs.

In this work, we demonstrate high performance PSCs by employing as-prepared zirconium acetylacetonate film (a-ZrAcac) as CBL. The a-ZrAcac CBL was simply prepared by spin-coating its ethanol solution on photoactive layer at room temperature, no thermal annealing or any other post-treatment was performed. To investigate the photovoltaic performance of the a-ZrAcac CBL, bulk-heterojunction PSCs based on P3HT (poly(3-hexylthiophene)) or low bandgap D-A copolymer PBT1 (poly(1,3-bis(2-ethylhexyl)-5,7-bis(4-(2-ethylhex-

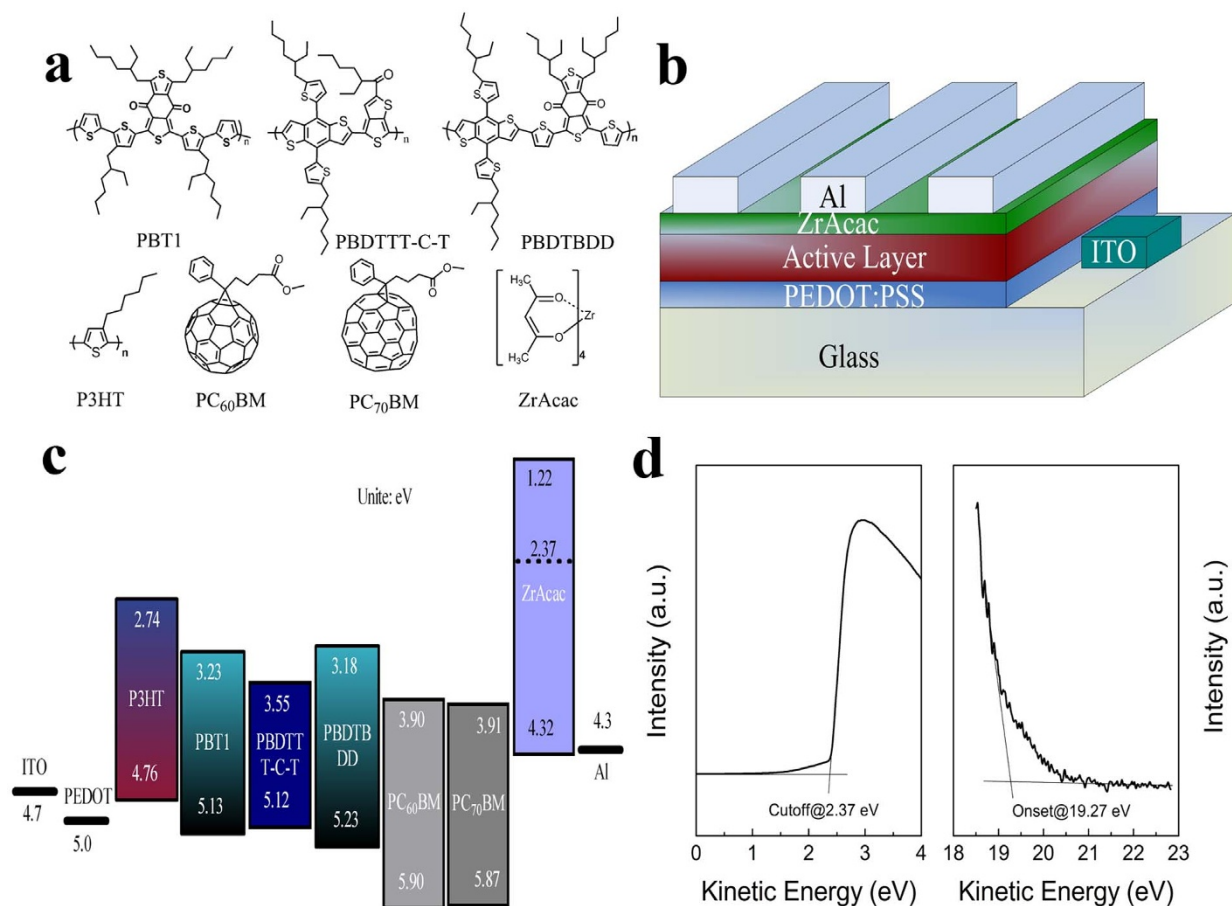


**Figure 1** | (a) Molecular structures of P3HT, PBT1, PBDTBD-C-T, PBDTBDD, PC<sub>60</sub>BM, PC<sub>70</sub>BM and ZrAcac; (b) Device structure of the polymer solar cells; (c) Schematic energy diagram of the materials involved in the PSCs; (d) UPS spectra of a-ZrAcac on ITO substrate.

yl)thiophen-2-yl)benzo[1,2-c : 4,5-c']dithiophene-4,8-dione)-co-(2,2'-bithiophene)), PBDTTT-C-T (poly(4,8-bis(5-(2-ethylhexyl)thiophen-2-yl)-benzo[1,2-b : 4,5-b']dithiophene-alt -alkylcarbonylthieno[3,4-b]thiophene)), and PBDTBDD (poly(((4,8-Bis(5-(2-ethylhexyl)thiophen-2-yl)benzo[1,2-b : 4,5-b']dithiophene-2,6-diyl)bis(trimethyl))-co-(5,7-bis(2-ethylhexyl)benzo[1,2-c : 4,5-c']dithiophene-4,8-dione))) as electron donor and PC<sub>60</sub>BM or PC<sub>70</sub>BM as electron acceptor were fabricated with a-ZrAcac/Al as cathode. The molecular structures of donor, acceptor and ZrAcac are shown in Figure 1(a). The power conversion efficiency (PCE) of the P3HT:PC<sub>60</sub>BM-based device with a-ZrAcac CBL reaches 4.23%, which is nearly 60% increased in comparison with the PSC without the buffer layer and ca. 12% increased than that of the PSC with traditional Ca/Al cathode. For the PSCs with low bandgap polymer PBDTBDD as electron donor, an average PCE of 8.75% with a maximum of 9.23% was achieved with a-ZrAcac CBL, greatly improved in comparison to the devices with Al (5.72%) or Ca/Al (7.34%) as cathode.

## Results

The a-ZrAcac layer is highly transparent in the visible wavelength range as shown in Figure S1 in Supporting Information (SI) and bearing an amorphous structure confirmed by XRD (Figure S2 in SI). The characteristic absorption peak of acetylacetonate located at 300 nm attributes to the  $n-\pi^*$  and  $\pi-\pi^*$  intra-ligand electronic transitions<sup>37,38</sup>. The transparency of the a-ZrAcac layer will benefit the transmission and reflection on the back Al electrode for the transmitted light through the active layer, which will potentially increase the light harvest of the photoactive layer and thus enhance the photocurrent of the PSCs. a-ZrAcac possesses a high stability constant<sup>39</sup>

and is thermally stable at lower than 150°C as shown in the thermogravimetric analysis (TGA) and differential thermal analysis (DTA) plots in Figure S3 in SI. Our result is in good agreement with previous study<sup>40</sup>.

The effects of a-ZrAcac CBL on the photovoltaic performance of PSCs were examined by constructing the traditional structured devices of ITO/PEDOT:PSS/Active layer/a-ZrAcac/Al, as shown in Figure 1(b). In the PSCs, the active layer is P3HT:PC<sub>60</sub>BM, P3HT:PC<sub>70</sub>BM, PBT1:PC<sub>70</sub>BM, PBDTTT-C-T:PC<sub>70</sub>BM or PBDTBDD:PC<sub>60</sub>BM blend film, PEDOT:PSS is poly(3,4-ethylenedioxythiophene):poly(styrenesulfonate). Figure 1(c) shows the highest occupied molecular orbital (HOMO) and the lowest unoccupied molecular orbital (LUMO) energy levels of P3HT<sup>41</sup>, PBDTBDD<sup>42</sup>, PBT1<sup>43</sup>, PBDTTT-C-T<sup>44</sup>, PC<sub>60</sub>BM<sup>45</sup>, PC<sub>70</sub>BM<sup>46</sup> and a-ZrAcac, where the energy levels of ZrAcac were measured by ultraviolet photoelectron spectroscopy (UPS). Figure 1(d) illustrates the UPS spectra taken from the ZrAcac coated on ITO substrate. The work function can be deduced from the energy of the secondary cutoff, which is 2.37 eV. The HOMO level can be calculated as 4.32 eV from the difference between the incident light energy (He I, 21.22 eV) and the energy of the onset (19.27 eV) as well as the work function. The LUMO level of 1.22 eV was obtained from the band gap of 3.1 eV (determined from onset of the absorption (400 nm) (see Figure S1 in SI)) and the HOMO level. The energy level alignment at the photoactive blend layer/a-ZrAcac interface is very important for high performance PSCs. The extremely low work function of ZrAcac (2.37 eV) lies above the LUMO energy levels of PC<sub>60</sub>BM (3.90 eV) and PC<sub>70</sub>BM (3.91 eV), inducing the interfacial dipole formation across this interface, which will facilitate “barrier-free” electron extraction from the LUMOs of PC<sub>60</sub>BM and



PC<sub>70</sub>BM<sup>47</sup>. The good energy level matching of ZrAcac can expect excellent electron extraction from photoactive layer and enhanced performance of the PSCs.

Surface morphology of a-ZrAcac layer spin-coated on clean ITO glass surface was investigated by tapping-mode atomic force microscopy (AFM), as shown in Figure S4 in SI. The AFM image shows a root-mean-square (rms) roughness of 3.4 nm, which is a little lower than that (4.6 nm) of bare ITO surface as shown in Figure S5. The surface morphologies of the photoactive layer with and without a-ZrAcac CBL were also investigated by AFM, as illustrated in Figure 2. The rms roughness of the blend layer of P3HT:PC<sub>60</sub>BM is 16.9 nm (Figure 2(a)), while the surface covered by the a-ZrAcac layer becomes more rough with a rms of 19.6 nm (Figure 2(b)). The same roughness changing trend but smaller roughness was observed for the blend layers of PBDTBDD:PC<sub>60</sub>BM. The rms roughness of the blend layers of PBDTBDD:PC<sub>60</sub>BM with and without a-ZrAcac CBL is 5.5 nm (Figure 2(d)) and 2.7 nm (Figure 2(c)), respectively. The increased roughness for the active layers with a-ZrAcac CBL could increase the contact area with the Al electrode deposited on it<sup>48</sup>.

The chemical component of ZrAcac powder and as prepared ZrAcac layer (a-ZrAcac, 40 nm) on glass slide was analyzed by X-ray photoelectron spectroscopy (XPS) as shown in Figure 3. The binding energies (BE) obtained in the XPS analysis are corrected for specimen charge by referencing the C 1 s peak to 284.8 eV. As shown in Figure 3(a), the survey scan for both powder and thin film samples performed in the 0–1000 eV BE range show characteristic peaks of the elements Zr, O, and C. As shown in Figure 3(b), the XPS spectrum of the core level of Zr 3d for the powder sample has a strong spin–orbit doublet due to Zr 3d<sub>5/2</sub> at 182.3 eV and Zr 3d<sub>3/2</sub> at 184.7 eV<sup>49,50</sup>. The XPS spectrum is constrained by the Zr 3d<sub>5/2</sub>–Zr 3d<sub>3/2</sub> spin–orbit separation being 2.4 eV, and the area ratio of the two

peaks of each doublet being 3 : 2. These features are characteristic of Zr<sup>4+</sup> ions in full oxidation states<sup>49,50</sup>. In the XPS spectrum of the a-ZrAcac thin film sample, the peaks corresponding to Zr 3d<sub>5/2</sub> and Zr 3d<sub>3/2</sub> are unchanged at 182.3 eV and 184.7 eV, respectively, with an Zr 3d<sub>5/2</sub>–Zr 3d<sub>3/2</sub> spin–orbit separation of 2.4 eV and an intensity ratio of 3 : 2. The results indicate that the zirconium in the thin film sample is also in the Zr<sup>4+</sup> oxidation state. The O 1 s XPS spectra for the powder and thin film samples are shown in Figure 3(c). It can be observed that the original powder sample presents nonsymmetric O 1 s peak centered at 531.3 eV with a shoulder around 530 eV. The peak at 531.3 eV corresponds to the oxygen in the acetylacetonate ligand cycle<sup>30</sup>, while the shoulder at 530 eV should attribute to the oxygen bonded with zirconium<sup>49,50</sup>, which means there is a small portion (17% from the peak fitting) of Zr<sup>4+</sup> ions coordinate less than four acetylacetonate ligands in the original powder sample and this is a common case in coordination complexes<sup>51</sup>. The thin film sample shows similar O 1 s peak, and the portion of non-four-coordination is 15%, which means there is no decomposition occurred. As shown in Figure 3(d), the C 1 s peaks of ZrAcac powder are located at 284.7 eV, which is assigned to the carbon in C–H/C–C group<sup>52</sup>, the peak at 286.7 eV corresponds to the carbon in delocalized C=O of ligand cycle<sup>52</sup>, and the weak shoulder at 288.3 eV attributes to the absorbed CO<sub>2</sub> from ambient atmosphere<sup>52</sup>. The atomic ratio of C 1 s (286.7 eV) and C 1 s (284.7 eV) peaks is 1 : 3.50, which is very close to the ratio of 1 : 3.54 for thin film sample. The XPS results confirm that there is no structure change between the powder and the obtained thin film.

Figure 4 shows current density–voltage (*J*–*V*) curves of the PSCs based on P3HT:PC<sub>60</sub>BM, PBDTBDD:PC<sub>60</sub>BM, P3HT:PC<sub>70</sub>BM, PBT1:PC<sub>70</sub>BM and PBDTTT–C–T:PC<sub>70</sub>BM with different cathode in the dark and under the illumination of AM 1.5 G, 100 mW/cm<sup>2</sup>.

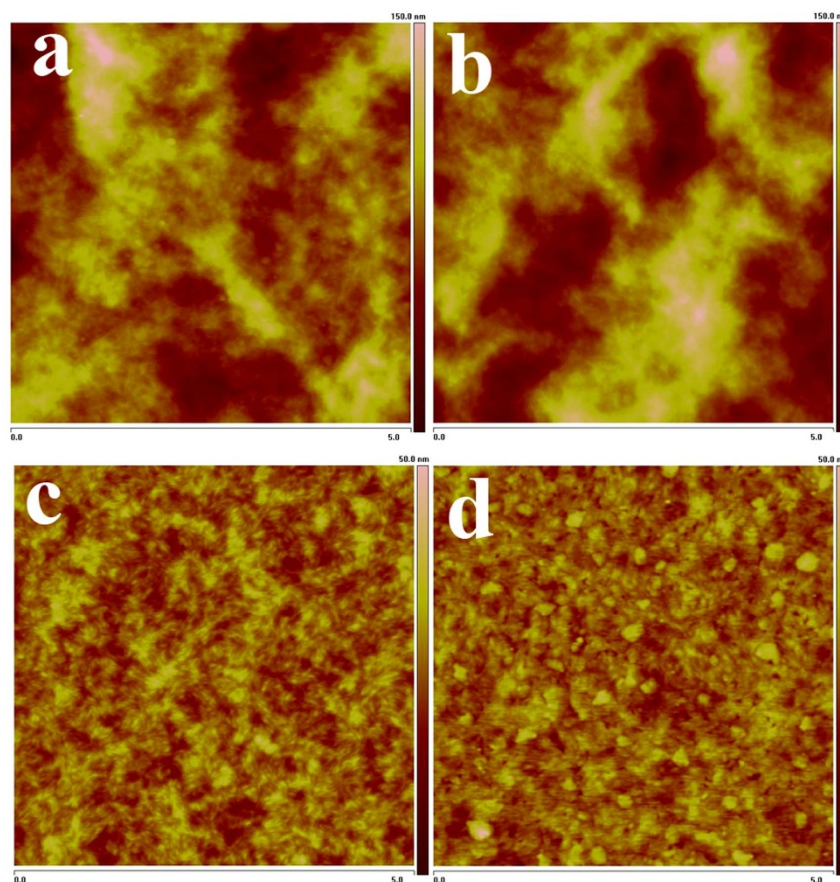


**Figure 2** | AFM images of P3HT:PC<sub>60</sub>BM blend film on ITO/PEDOT:PSS substrate without (a) and with (b) a-ZrAcac layer, and AFM images of PBDTBDD:PC<sub>60</sub>BM blend film on ITO/PEDOT:PSS substrate without (c) and with (d) a-ZrAcac layer. The scan size is 5 μm × 5 μm.

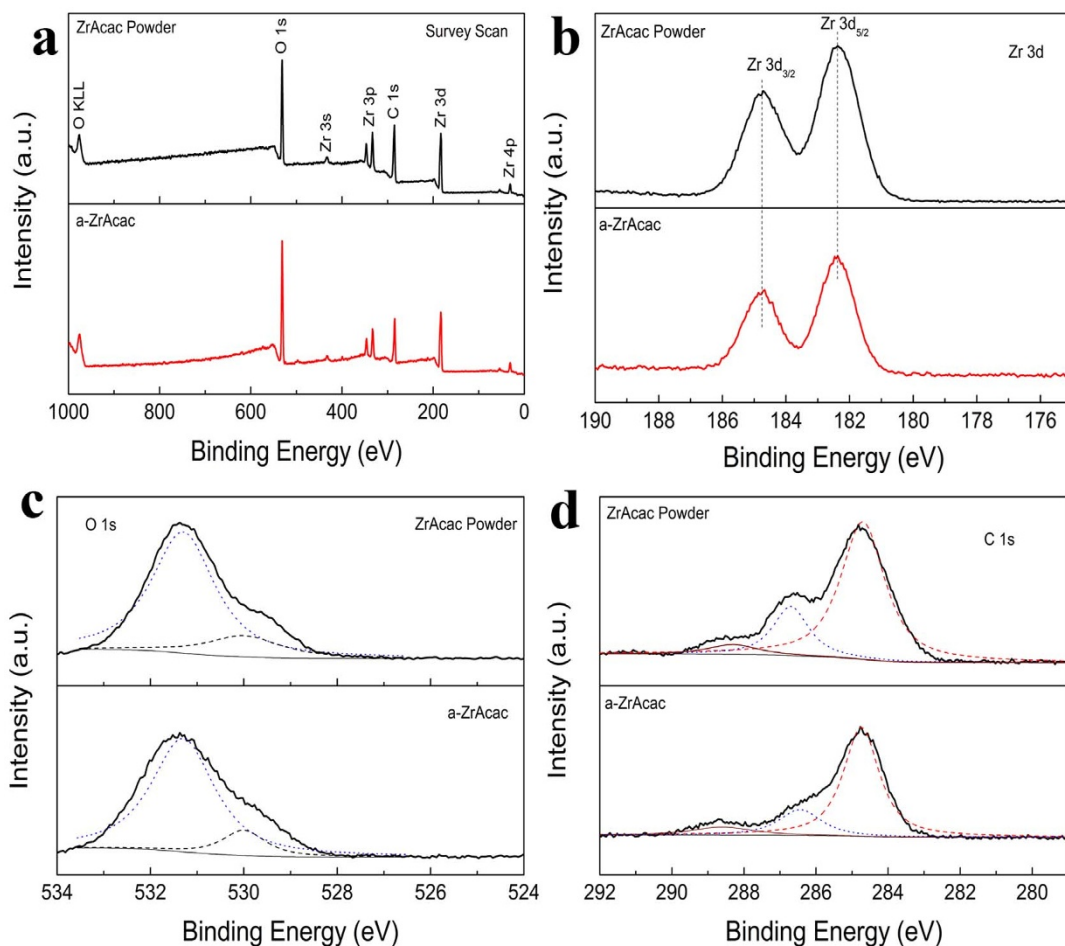


**Figure 3** | X-ray photoelectron spectroscopy (XPS) of ZrAcac powder and a-ZrAcac film (40 nm) on glass substrate. (a) survey scan, (b) Zr 3d, (c) O 1s, and (d) C 1s core level spectra.

The device performance parameters are given in Table 1, which are average values of 20 individual devices. For example, the  $V_{oc}$ ,  $J_{sc}$ , FF and PCE for PBDTBDD:PC<sub>60</sub>BM based on 20 devices are listed in Table S1 in SI. As shown in the inset of Figure 4(a), the  $J$ - $V$  curves measured in the dark for the PSCs based on P3HT:PC<sub>60</sub>BM show quite different charge injection and rectification behavior for the devices with different cathode. At positive bias of 1.5 V, the injection current of the device with Al cathode is 72.3 mA/cm<sup>2</sup>, with a rectification ratio of  $8.03 \times 10^3$  at  $\pm 1.5$  V. While that of the device with Ca/Al as cathode increased to 250.2 mA/cm<sup>2</sup> with a rectification ratio of  $1.39 \times 10^4$ . Interestingly, when utilizing a-ZrAcac/Al as cathode, the injection current is dramatically increased to 388.8 mA/cm<sup>2</sup> with a rectification ratio of  $3.09 \times 10^4$ , which is even much higher than that of the Ca/Al based device. The ZrAcac CBL works very well in PBDTBDD:PC<sub>60</sub>BM based devices, the injection current at 1.5 V and rectification ratio at  $\pm 1.5$  V for device with ZrAcac buffer layer (Figure 4(b) inset) reach 436.0 mA/cm<sup>2</sup> and  $9.91 \times 10^3$ , respectively, much higher than that of the PSCs with Ca/Al (275.9 mA/cm<sup>2</sup>,  $2.39 \times 10^3$ ) or Al (59.7 mA/cm<sup>2</sup>,  $1.90 \times 10^3$ ) as cathode. The enhanced charge injection and improved rectification ratio also can be seen in PC<sub>70</sub>BM based P3HT (Figure 4(c)) and low bandgap PBT1 (Figure 4(d)) and PBDTTT-C-T (Figure 4(e)) devices with a-ZrAcac CBL.

The PSCs based on P3HT:PC<sub>60</sub>BM with only Al cathode gives a PCE of 2.65%, with an open-circuit voltage ( $V_{oc}$ ) of 0.56 V, a short-circuit current density ( $J_{sc}$ ) of 9.55 mA/cm<sup>2</sup>, and a fill factor (FF) of 49.6%. In contrast, the four parameters of  $V_{oc}$ ,  $J_{sc}$ , FF, and PCE for the device with a-ZrAcac/Al cathode are all enhanced to 0.60 V, 10.66 mA/cm<sup>2</sup>, 66.1%, and 4.23%, respectively. The pho-

tovoltaic performance of the device with a-ZrAcac/Al cathode is also significantly improved than that of the device with traditional Ca/Al cathode with PCE increased by 12.8%. Furthermore, the a-ZrAcac CBL shows excellent performance in the PSCs based on low bandgap D-A copolymer PBDTBDD:PC<sub>60</sub>BM, as shown in Figure 4(b) and Table 1. The control device with only Al cathode shows a PCE of 5.72%, with a  $V_{oc}$  of 0.78 V, a  $J_{sc}$  of 12.10 mA/cm<sup>2</sup>, and an FF of 60.6%. With Ca/Al cathode, a similar  $J_{sc}$  is obtained, while both the  $V_{oc}$  and the FF are improved to 0.86 V and 70.8%, respectively, achieving an enhanced PCE of 7.34%. Surprisingly, the  $V_{oc}$ ,  $J_{sc}$  and PCE of the PSCs with a-ZrAcac/Al cathode are all greatly enhanced to 0.88 V, 14.28 mA/cm<sup>2</sup> and 8.75%, respectively. The best device shows a PCE of 9.23%, a  $V_{oc}$  of 0.89 V, a  $J_{sc}$  of 14.25 mA/cm<sup>2</sup>, and a FF of 72.7%, among the highest values reported in the literature so far for PSCs. For the significantly increased  $V_{oc}$  of the devices with Ca/Al or a-ZrAcac/Al cathode in comparison with that with Al cathode, it should be ascribed to the lower work function of Ca and ZrAcac compared with that of Al. In comparing the a-ZrAcac/Al based devices with the Ca/Al based devices, the improved PCE is mainly attributed to the enhanced  $J_{sc}$  and FF. The increased FF for the devices with a-ZrAcac/Al cathode could result from the enhanced charge extraction, increased light harvest and greatly decreased series resistance<sup>44</sup> (see Table 1). The series resistance ( $R_s$ ) of the PSCs based on P3HT:PC<sub>60</sub>BM is decreased from 13.0 ohm for Al cathode to 3.5 ohm for Ca/Al cathode and to 2.3 ohm for the a-ZrAcac/Al cathode, and that of the PSCs based on PBDTBDD:PC<sub>60</sub>BM is decreased from 11.5 ohm for Al cathode to 2.0 ohm for Ca/Al cathode and to 1.2 ohm for the a-ZrAcac/Al cathode.

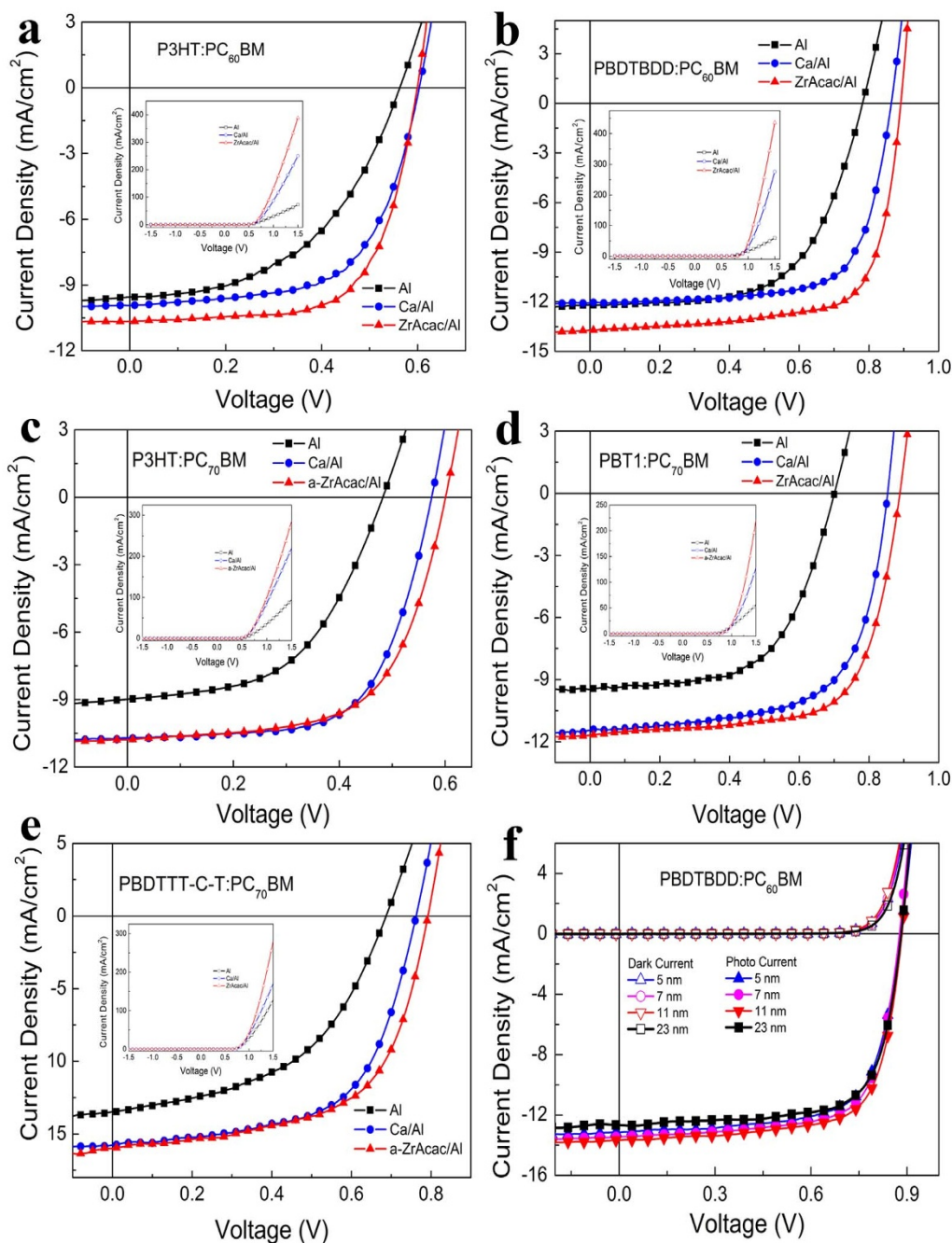


**Figure 4** |  $J-V$  curves under the illumination of AM 1.5 G,  $100 \text{ mW/cm}^2$  for the PSCs based on (a) P3HT:PC<sub>60</sub>BM, (b) PBDBTDD:PC<sub>60</sub>BM, (c) P3HT:PC<sub>70</sub>BM, (d) PBT1:PC<sub>70</sub>BM, and (e) PBDTTT-C-T:PC<sub>70</sub>BM with different cathode, insets are dark current at full bias scan from  $-1.5 \text{ V}$  to  $1.5 \text{ V}$ ; (f)  $J-V$  curves of the PSCs based on PBDBTDD:PC<sub>60</sub>BM with varied thickness of a-ZrAcac cathode buffer layer.

The a-ZrAcac CBL is of great compatibility with a variety of photoactive layers and shows good photovoltaic performance. As shown in Figure 4(c–e), with modified by a-ZrAcac layer, the PCE of the devices based on P3HT:PC<sub>70</sub>BM, PBT1:PC<sub>70</sub>BM, and PBDTTT-C-T:PC<sub>70</sub>BM reaches 4.01%, 7.06%, and 7.55%, respectively, increased by 42%, 80%, and 66%, in comparison with the devices with bare Al cathode. It's also higher than that (3.88%, 6.34% and 7.22%, respectively) of the devices with Ca/Al electrodes. Comparing the performance of PC<sub>70</sub>BM based devices, the enhanced PCE for a-ZrAcac buffered devices can mainly attributed to the enhanced  $V_{oc}$ , since the  $J_{sc}$  and FF is similar to the devices with Ca/Al cathodes. The improved  $V_{oc}$  should attribute to the interfacial dipoles<sup>47</sup> formed by inserting a-ZrAcac layer as shown in Figure 1(c).

The  $J-V$  curves of PBDBTDD:PC<sub>60</sub>BM and P3HT:PC<sub>60</sub>BM based devices with varied a-ZrAcac thickness are shown in Figure 4(f) and Figure S6, respectively, and the parameters of the devices are summarized in Table S2 and Table S3 in SI, respectively. The  $J_{sc}$  is insensitive to a-ZrAcac layer thickness in a wide thickness range, while the overall performance critically depends on its thickness, because a too thick interfacial layer will induce a high series resistance, while a too-thin layer could not provide an ohmic contact for electron extraction.

## Discussion

In order to further elucidate the increased  $J_{sc}$  for the devices with a-ZrAcac CBL, we compared the external quantum efficiency (EQE)



**Table 1 | Device parameters of the PSCs based on P3HT:PC<sub>60</sub>BM, PBDBTDD:PC<sub>60</sub>BM, P3HT:PC<sub>70</sub>BM, PBT1:PC<sub>70</sub>BM and PBDDTT-C-T:PC<sub>70</sub>BM with different cathode under the illumination of AM 1.5 G, 100 mW/cm<sup>2</sup>**

Active Layer	Cathode	V <sub>oc</sub> (V)	J <sub>sc</sub> (mA/cm <sup>2</sup> )	FF (%)	PCE (%)	R <sub>s</sub> <sup>[a]</sup> (Ω cm <sup>2</sup> )
P3HT:PC <sub>60</sub> BM	Al	0.56	9.55	49.6	2.65	13.0
	Ca/Al	0.60	9.95	62.8	3.75	3.5
	α-ZrAcac/Al	0.60	10.66	66.1	4.23	2.3
PBDBTDD:PC <sub>60</sub> BM	Al	0.78	12.10	60.6	5.72	11.5
	Ca/Al	0.86	12.06	70.8	7.34	2.0
	α-ZrAcac/Al	0.88	14.28	69.6	8.75	1.2
P3HT:PC <sub>70</sub> BM	Al	0.55	9.11	56.5	2.83	8.9
	Ca/Al	0.58	10.71	62.5	3.88	3.8
	α-ZrAcac/Al	0.60	10.73	62.3	4.01	2.8
PBT1:PC <sub>70</sub> BM	Al	0.70	9.50	58.9	3.92	12.4
	Ca/Al	0.86	11.44	64.4	6.34	5.1
	α-ZrAcac/Al	0.88	11.68	68.7	7.06	3.2
PBDDTT-C-T:PC <sub>70</sub> BM	Al	0.68	13.47	49.7	4.55	5.4
	Ca/Al	0.76	15.76	60.3	7.22	4.0
	α-ZrAcac/Al	0.79	15.95	60.0	7.55	2.4

<sup>[a]</sup>Series resistance (R<sub>s</sub>) of the PSCs in the dark are obtained at around 1.2 V.

spectra of the PSCs with Al, Ca/Al and α-ZrAcac/Al cathodes, as given in Figure 5(a) (PBDBTDD:PC<sub>60</sub>BM based devices) and Figure S7 (P3HT:PC<sub>60</sub>BM based devices) in SI. As shown in Figure 5(a), in comparison with the devices with Al and Ca/Al cathode, the EQE spectra of PSCs based on PBDBTDD:PCBM with α-ZrAcac CBL exhibits enhanced light response in the whole absorption band of 300–700 nm, giving a notable enhancement in wavelength range from 380 nm to 500 nm, where it is a deep valley for the devices with Al and Ca/Al cathode due to the limited absorption of the polymer as shown in Figure S8 in SI.

To further clarify the different light response behavior, we measured the reflectance spectra of the devices with Al and α-ZrAcac/Al cathode. As shown in Figure 5(b), the reflectance of the device with α-ZrAcac/Al cathode is lower than that of the device with only Al cathode in the wavelength range of 400–650 nm. Actually, the highly transparent characteristic and appropriate thickness of the α-ZrAcac layer could be its advantage on the reflectance over Ca or other organic CBL. To investigate the relationship between the enhanced light harvest (reduced light reflectance) and the increased EQE values (photocurrent response), we derived the additional absorption,  $\Delta\alpha_{Abs}$ , and the additional EQE,  $\Delta\alpha_{EQE}$ , from the reflectance and the EQE spectra, respectively, where  $\Delta\alpha_{Abs} = -\ln(\text{Ref}_{ZrAcac/Al}/\text{Ref}_{Al})$ , and  $\Delta\alpha_{EQE} = -\ln(\text{EQE}_{ZrAcac/Al}/\text{EQE}_{Al})$ . Figure 5(c) shows the  $\Delta\alpha_{Abs}$  and  $\Delta\alpha_{EQE}$  curves as the function of wavelength. It can be seen that the shape of  $\Delta\alpha_{EQE}$  curve is very similar to that of the  $\Delta\alpha_{Abs}$  curve, indicating that the enhanced photocurrent in the device with α-ZrAcac/Al cathode can be mainly ascribed to the additional absorption of the photoactive layer in the device.

To gain further insight into the origin of the enhanced J<sub>sc</sub> in the device, one-dimensional transfer matrix formalism<sup>53</sup> based on optical modelling calculations was conducted, where experimentally measured refractive indices and extinction coefficients were used. The exciton generation rate versus position in the PBDBTDD:PC<sub>60</sub>BM active layer (100 nm) is shown in Figure 6(a) for devices with Ca/Al and α-ZrAcac/Al cathode, verifying that the device with α-ZrAcac/Al cathode can generate more carriers than that of the Ca/Al based device, which accounts in part for the higher J<sub>sc</sub> of the device with α-ZrAcac/Al cathode. The calculated exciton generation rate is in good agreement with EQE measurement as shown in Figure 5(a). The normalized modulus of the optical electric field is shown in Figure 6(b) for the PSCs with an active layer thickness of 100 nm and with Ca/Al and α-ZrAcac/Al cathode for a wavelength of 430 nm. This wavelength has been chosen as the difference in EQE, and absorption between the two device stacks is most prominent at 430 nm. Modified with α-ZrAcac causes little shift of the

maximum of the electric field but greatly increases the overall modulus throughout the whole active layer. The calculated results of enhanced light distribution within the active layer for α-ZrAcac based device is in agreement with tested reflection spectra as shown in Figure 5(b).

The long term stability of non-encapsulated P3HT:PC<sub>60</sub>BM based PSCs with α-ZrAcac/Al and Ca/Al cathodes were investigated by testing the evolution of the characteristic parameters (V<sub>oc</sub>, J<sub>sc</sub>, FF, and PCE) with time in a nitrogen filled glove-box (the concentration of H<sub>2</sub>O and O<sub>2</sub> is less than 20 ppm) as shown in Figure 7. After 720 hours (30 days), the PCEs of the devices with Ca/Al drop to about 56% of the initial PCEs. The observed decrease in the PCE is mainly due to a deterioration of both J<sub>sc</sub> and FF, with a little drop (5%) of V<sub>oc</sub>. On the contrary, the devices with α-ZrAcac/Al cathodes were found to show dramatically improved stability and after 30 days retained 93% of its initial PCE under N<sub>2</sub>. This is in excellent agreement with the stability of PSCs using solution processed PFN layers reported previously<sup>32</sup>. These results indicate that the α-ZrAcac interfacial layer can effectively improve the long term stability of PSCs.

In summary, we successfully demonstrate high performance PSCs by employing as-prepared ZrAcac film spin-cast from its ethanol solution as CBL. The devices with α-ZrAcac/Al cathode show decreased series resistance and enhanced photocurrent due to the remarkable improvement of the charge extraction and light harvesting. The PCE of the device based on P3HT:PC<sub>60</sub>BM with α-ZrAcac CBL reaches 4.23% under the illumination of AM1.5G 100 mW/cm<sup>2</sup>. When choosing D-A copolymer PBDBTDD as electron donor, an average PCE of 8.75% and a best PCE of 9.23% was achieved, which is greatly improved (19% enhancement) in comparison with that (7.34%) of the device with traditional Ca/Al cathode. Our findings indicate that α-ZrAcac is a promising CBL for the fabrication of large area flexible PSCs.

## Methods

**Device fabrication and characterization.** The ITO glass (sheet resistance: 10 Ω/sq, CSG Holding, China) was sequential ultrasonic cleaned in detergent, deionized water, acetone, and isopropanol, and then treated in an ultraviolet-ozone chamber (Jelight, USA) for 20 min. PEDOT:PSS (Clevious P VP AI 4083, H. C. Stark) aqueous solution was filtered through a 0.45 μm filter and spin-coated at 2000 rpm for 60 s on the pre-treated ITO substrate, followed by 150°C baking for 10 min in air, achieving a 30 nm thick PEDOT:PSS layer. Subsequently, the PEDOT:PSS modified substrate was transferred to a nitrogen-filled glove-box for photoactive layer and cathode buffer layer preparation. The P3HT (Rieke Metals) and PC<sub>60</sub>BM or PC<sub>70</sub>BM (Nano-C) blend layer was prepared by spin-coating (800 rpm) the 1, 2-dichlorobenzene (ODCB) solution of P3HT and PC<sub>60</sub>BM or PC<sub>70</sub>BM (1:1 w/w, polymer concentration of 20 mg/mL) on the PEDOT:PSS modified ITO electrode for 20 s, followed by solvent-annealing<sup>54</sup> in covered glass Petri dish, obtaining a 240 nm thick

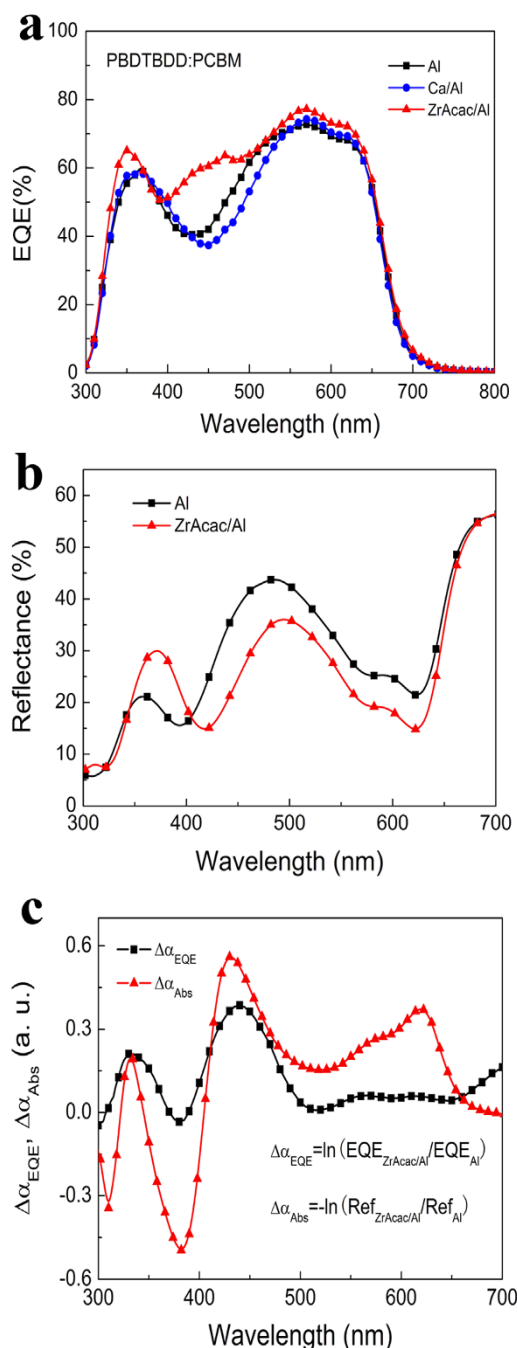


**Figure 5** | (a) External quantum efficiency (EQE) spectra, and (b) the reflectance spectra of the PSCs based on PBDTBDD:PC<sub>60</sub>BM with different cathode; (c) the additional absorption spectrum as well as additional EQE spectrum calculated from the difference of reflectance spectra and EQE spectra of the PSCs based on PBDTBDD:PC<sub>60</sub>BM with a-ZrAcac/Al and Al cathode, respectively.

photoactive layer. The PBDTBDD and PC<sub>60</sub>BM blend photoactive layer was prepared by spin-coating (1200 rpm) the dichlorobenzene solution of the mixed solution (1 : 1 w/w, polymer concentration of 15 mg/mL) with 3% volume ratio of 1,8-Diiodooctane (DIO, Sigma Aldrich) on the PEDOT:PSS modified ITO electrode. The thickness of the photoactive layer is about 100 nm. The PBT1 : PC<sub>70</sub>BM blend photoactive layer was prepared by spin-coating (800 rpm) the ODCB solution of the mixed solution (1 : 1 w/w, polymer concentration of 10 mg/mL) with 1% volume ratio of DIO on the PEDOT:PSS modified ITO electrode for 60 s, obtaining a ca. 80 nm thick film. The PBDTTT-C-T : PC<sub>70</sub>BM blend film was fabricated by spin-coating (1500 rpm) the ODCB solution of the mixed solution (1 : 1.5 w/w, polymer concentration of 12.5 mg/mL) with 3 vol% DIO on the ITO/PEDOT:PSS electrode for 60 s, yielding a ca. 80 nm thick photoactive layer. The ZrAcac powder was bought from Alfa Aesar with a purity of 98%. The ZrAcac ethanol solution was simply made by adding the ZrAcac powder

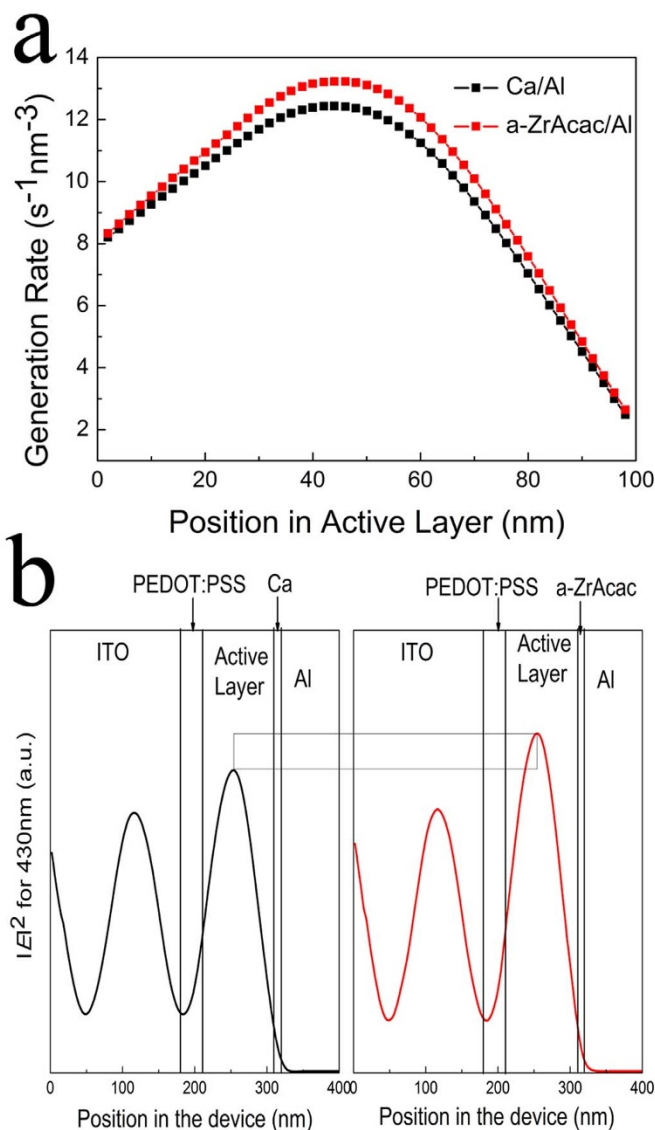


**Figure 6** | (a) Modeled exciton generation rate in the PBDTBDD:PC<sub>60</sub>BM active layer (100 nm) as a function of position within the active layer with Ca/Al and a-ZrAcac/Al cathode. (b) Calculated distribution of the normalized modulus squared of the optical electric field  $|E|^2$  inside a photovoltaic device: ITO (~180 nm)/PEDOT (~30 nm)/PBDTBDD:PC<sub>60</sub>BM (~100 nm)/Ca (10 nm) or a-ZrAcac (11 nm)/Al (90 nm) for a wavelength of 430 nm.

into the anhydrous ethanol solvent then stirred for 3 h, obtaining a colorless solution with concentration of 0.25–2 mg/mL. The ZrAcac cathode buffer layer was prepared by directly spin-coating (1500–6000 rpm) the ZrAcac ethanol solution on the photoactive layer for 60 s to obtain the film with different thickness, no any additional thermal annealing or post-treatment was performed. The just prepared ZrAcac thin layer named as a-ZrAcac layer. Finally, the substrate was transferred to a vacuum chamber and the metal cathode (Al or Ca/Al) was thermally deposited. The photoactive area of the device is around 4 mm<sup>2</sup> defined by perpendicular ITO and cathode electrode. The current density–voltage (*J*–*V*) and the external quantum efficiency measurements were conducted according to our previous publication<sup>30</sup>.

**Instrumentation.** The surface morphologies of the P3HT:PC<sub>60</sub>BM and PBDTBDD:PC<sub>60</sub>BM photoactive layers with and without ZrAcac layer were analyzed using a VEECO DICP-II atomic force microscope (AFM) operated in the tapping mode under ambient atmosphere at room temperature. The reflectance spectra were measured by LAMBDA 950 UV/Vis/NIR Spectrophotometer with the device structures of ITO/PEDOT:PSS/PBDTBDD:PC<sub>60</sub>BM/Al and ITO/PEDOT:PSS/PBDTBDD:PC<sub>60</sub>BM/a-ZrAcac/Al. The thickness of the photoactive layer was measured by Ambios Technology XP-2 surface profilometer. An ESCA Lab220i-XL electron spectrometer from VG Scientific using 300 W Al *K*  $\alpha$  radiation operated at a base pressure of  $3 \times 10^{-9}$  mbar was used to obtain XPS data. The

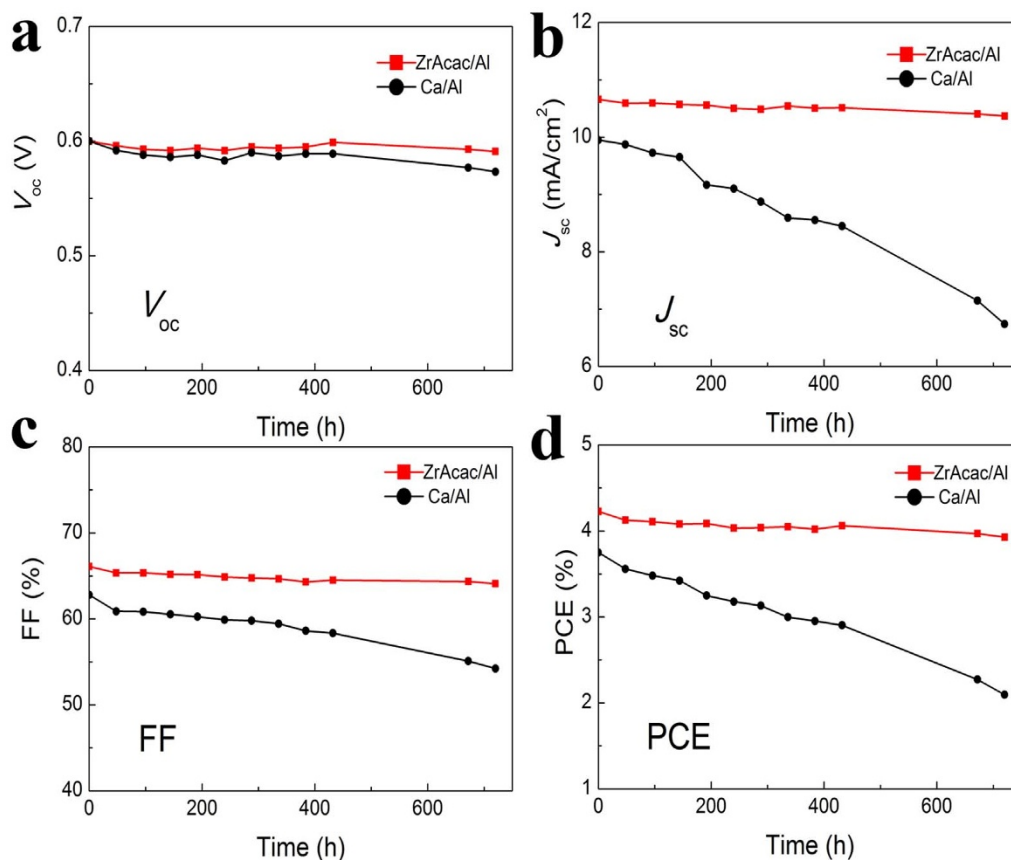


**Figure 7 | Long-term stability of the P3HT:PC<sub>60</sub>BM based PSCs with Ca/Al or a-ZrAcac/Al cathode.** The evolution of (a)  $V_{oc}$ , (b)  $J_{sc}$ , (c) FF, and (d) PCE with time. The devices were stored in an N<sub>2</sub> filled glove-box.

binding energies were referenced to adventitious carbon (C 1 s line at 284.8 eV). The ultraviolet photoelectron spectroscopy (UPS) measurements were conducted in ultra-high vacuum ( $3.0 \times 10^{-8}$  Torr) with a Kratos Axis Ultra DLD ultraviolet photoelectron spectrometer equipped with a monochromatic He ultraviolet source He I ( $h\nu = 21.22$  eV). To separate the sample and the secondary edge for the analyzer, a sample bias of  $-9$  V was applied. The optical constants of a-ZrAcac and the photoactive blend were derived from spectroscopic ellipsometry by SENTECH SE400 rotating compensator ellipsometer.

- Sariciftci, N. S., Smilowitz, L., Heeger, A. J. & Wudl, F. Photoinduced electron transfer from a conducting polymer to buckminsterfullerene. *Science* **258**, 1474–1476 (1992).
- Li, Y. F. Molecular design of photovoltaic materials for polymer solar cells: Toward suitable electronic energy levels and broad absorption. *Acc. Chem. Res.* **45**, 723–733 (2012).
- Chen, J. & Cao, Y. Development of novel conjugated donor polymers for high-efficiency bulk-heterojunction photovoltaic devices. *Acc. Chem. Res.* **42**, 1709–1718 (2009).
- Gunes, S., Neugebauer, H. & Sariciftci, N. S. Conjugated polymer-based organic solar cells. *Chem. Rev.* **107**, 1324–1338 (2007).
- Scharber, M. C. *et al.* Design rules for donors in bulk-heterojunction solar cells—Towards 10% energy-conversion efficiency. *Adv. Mater.* **18**, 789–794 (2006).
- Li, G., Zhu, R. & Yang, Y. Polymer solar cells. *Nat. Photonics* **6**, 153–161 (2012).
- Ma, H., Yip, H.-L., Huang, F. & Jen, A. K.-Y. Interface engineering for organic electronics. *Adv. Funct. Mater.* **20**, 1371–1388 (2010).
- Steim, R., Kogler, F. R. & Brabec, C. J. Interface materials for organic solar cells. *J. Mater. Chem.* **20**, 2499–2512 (2010).
- Chen, L.-M., Hong, Z., Li, G. & Yang, Y. Recent progress in polymer solar cells: manipulation of polymer:fullerene morphology and the formation of efficient inverted polymer solar cells. *Adv. Mater.* **21**, 1434–1449 (2009).
- Brabec, C. J. *et al.* Origin of the open circuit voltage of plastic solar cells. *Adv. Funct. Mater.* **11**, 374–380 (2001).
- Jørgensen, M., Norrman, K. & Krebs, F. C. Stability/degradation of polymer solar cells. *Sol. Energ. Mat. Sol. C.* **92**, 686–714 (2008).
- Kawano, K. *et al.* Degradation of organic solar cells due to air exposure. *Sol. Energ. Mat. Sol. C.* **90**, 3520–3530 (2006).
- Norrman, K., Gevorgyan, S. A. & Krebs, F. C. Water-induced degradation of polymer solar cells studied by H<sub>2</sub><sup>18</sup>O labeling. *ACS Appl. Mater. Interfaces* **1**, 102–112 (2009).

- Voroshazi, E. *et al.* Influence of cathode oxidation via the hole extraction layer in polymer:fullerene solar cells. *Org. Electron.* **12**, 736–744 (2011).
- Brabec, C. J., Shaheen, S. E., Winder, C., Sariciftci, N. S. & Denk, P. Effect of LiF/metal electrodes on the performance of plastic solar cells. *Appl. Phys. Lett.* **80**, 1288 (2002).
- Li, G., Chu, C.-W., Shrotriya, V., Huang, J. & Yang, Y. Efficient inverted polymer solar cells. *Appl. Phys. Lett.* **88**, 253503 (2006).
- Liao, H.-H., Chen, L.-M., Xu, Z., Li, G. & Yang, Y. Highly efficient inverted polymer solar cell by low temperature annealing of Cs<sub>2</sub>CO<sub>3</sub> interlayer. *Appl. Phys. Lett.* **92**, 173303 (2008).
- Yip, H.-L., Hau, S. K., Baek, N. S., Ma, H. & Jen, A. K.-Y. Polymer solar cells that use self-assembled-monolayer-modified ZnO/metals as cathodes. *Adv. Mater.* **20**, 2376–2382 (2008).
- Yip, H. L., Hau, S. K., Baek, N. S. & Jen, A. K. Y. Self-assembled monolayer modified ZnO/metal bilayer cathodes for polymer/fullerene bulk-heterojunction solar cells. *Appl. Phys. Lett.* **92**, 193313 (2008).
- Kim, J. Y. *et al.* Solution-processable zinc oxide for the polymer solar cell based on P3HT:PCBM. *Nanosci. Nanotechnol.* **11**, 5995–6000 (2011).
- Jo, S. B. *et al.* High performance organic photovoltaic cells using polymer-hybridized ZnO nanocrystals as a cathode interlayer. *Adv. Energy Mater.* **1**, 690–698 (2011).
- Kim, J. Y. *et al.* New architecture for high-efficiency polymer photovoltaic cells using solution-based titanium oxide as an optical spacer. *Adv. Mater.* **18**, 572–576 (2006).
- Park, S. H. *et al.* Bulk heterojunction solar cells with internal quantum efficiency approaching 100%. *Nat. Photonics* **3**, 297–302 (2009).
- Sun, Y. *et al.* Efficient, air-stable bulk heterojunction polymer solar cells using MoO<sub>x</sub> as the anode interfacial layer. *Adv. Mater.* **23**, 2226–2230 (2011).
- Salim, T. *et al.* Solution-processed nanocrystalline TiO<sub>2</sub> buffer layer used for improving the performance of organic photovoltaics. *ACS Appl. Mater. Interfaces* **3**, 1063–1067 (2011).
- Tan, Z. A., Yang, C. H., Zhou, E. J., Wang, X. & Li, Y. F. Performance improvement of polymer solar cells by using a solution processible titanium chelate as cathode buffer layer. *Appl. Phys. Lett.* **91**, 023509 (2007).
- Wang, F. Z. *et al.* Alcohol soluble titanium(IV) oxide bis(2,4-pentanedionate) as electron collection layer for efficient inverted polymer solar cells. *Org. Electron.* **13**, 2429–2435 (2012).
- Zhang, W. Q. *et al.* ITO electrode/photoactive layer interface engineering for efficient inverted polymer solar cells based on P3HT and PCBM using a solution-processed titanium chelate. *J. Phys. D: Appl. Phys.* **45**, 285102 (2012).





29. Wang, F. Z. *et al.* Improved performance of polymer solar cells based on P3HT and ICBA using alcohol soluble titanium chelate as electron collection layer. *Org. Electron.* **14**, 845–851 (2013).
30. Tan, Z. A. *et al.* High-performance inverted polymer solar cells with solution-processed titanium chelate as electron-collecting layer on ITO electrode. *Adv. Mater.* **24**, 1476–1481 (2012).
31. He, Z. *et al.* Simultaneous enhancement of open-circuit voltage, short-circuit current density, and fill factor in polymer solar cells. *Adv. Mater.* **23**, 4636–4643 (2011).
32. He, Z. *et al.* Enhanced power-conversion efficiency in polymer solar cells using an inverted device structure. *Nat. Photonics* **6**, 591–595 (2012).
33. Lv, M. *et al.* A hyperbranched conjugated polymer as the cathode interlayer for high-performance polymer solar cells. *Adv. Mater.* **25**, 6889–6894 (2013).
34. Tokmoldin, N., Griffiths, N., Bradley, D. D. C. & Haque, S. A. A hybrid inorganic–organic semiconductor light-emitting diode using ZrO<sub>2</sub> as an electron-injection layer. *Adv. Mater.* **21**, 3475–3478 (2009).
35. Park, J. S. *et al.* High performance polymer light-emitting diodes with N-type metal oxide/conjugated polyelectrolyte hybrid charge transport layers. *Appl. Phys. Lett.* **99**, 163305 (2011).
36. Vasilopoulou, M. *et al.* Atomic layer deposited zirconium oxide electron injection layer for efficient organic light emitting diodes. *Org. Electron.* **14**, 312–319 (2013).
37. Li, Q., Zhong, X., Hu, J. & Kang, W. Preparation and corrosion resistance studies of zirconia coating on fluorinated AZ91D magnesium alloy. *Prog. Org. Coat.* **63**, 222–227 (2008).
38. Loukova, G. V., Huhn, W., Vasiliev, V. P. & Smirnov, V. Ligand-to-metal charge transfer excited states with unprecedented luminescence yield in fluid solution. *J. Phys. Chem. A* **111**, 4117–4121 (2007).
39. Stary, J. & Liljenzin, J. O. Critical evaluation of equilibrium constants involving acetylacetone and its metal chelates. *Pure Appl. Chem.* **54**, 2557–2592 (1982).
40. Ismail, H. M. Characterization of the decomposition products of zirconium acetylacetonate: nitrogen adsorption and spectrothermal investigation. *Powder Technol.* **85**, 253–259 (1995).
41. Hou, J. *et al.* Synthesis and photovoltaic properties of two-dimensional conjugated polythiophenes with bi(thienylenevinylene) side chains. *J. Am. Chem. Soc.* **128**, 4911–4916 (2006).
42. Qian, D. *et al.* Design, application, and morphology study of a new photovoltaic polymer with strong aggregation in solution state. *Macromolecules* **45**, 9611–9617 (2012).
43. Qian, D. *et al.* Molecular design toward efficient polymer solar cells with high polymer content. *J. Am. Chem. Soc.* **135**, 8464–8467 (2013).
44. Tan, Z. *et al.* Solution-processed rhenium oxide: a versatile anode buffer layer for high performance polymer solar cells with enhanced light harvest. *Adv. Energy Mater.* **4**, 1300884 (2014).
45. He, Y., Chen, H.-Y., Hou, J. & Li, Y. Indene–C<sub>60</sub> bisadduct: a new acceptor for high-performance polymer solar cells. *J. Am. Chem. Soc.* **132**, 1377–1382 (2010).
46. Tan, Z. *et al.* solution-processed tungsten oxide as an effective anode buffer layer for high-performance polymer solar cells. *J. Phys. Chem. C* **116**, 18626–18632 (2012).
47. Yip, H.-L. & Jen, A. K.-Y. Recent advances in solution-processed interfacial materials for efficient and stable polymer solar cells. *Energy Environ. Sci.* **5**, 5994–6011 (2012).
48. Ma, W., Yang, C., Gong, X., Lee, K. & Heeger, A. J. Thermally stable, efficient polymer solar cells with nanoscale control of the interpenetrating network morphology. *Adv. Funct. Mater.* **15**, 1617–1622 (2005).
49. Barreca, D. *et al.* Zirconium Dioxide Thin Films Characterized by XPS. *Surf. Sci. Spectra* **7**, 303–309 (2000).
50. Lung, C., Kukk, E., Hägerth, T. & Matinlinna, J. Surface modification of silica-coated zirconia by chemical treatments. *Appl. Surf. Sci.* **257**, 1228–1235 (2010).
51. Wilkinson, G., Gillard, R. D. & McCleverty, J. A. *Comprehensive coordination chemistry: The synthesis, reactions, properties & applications of coordination compounds.* Pergamon Press 1987.
52. Palmer, D. M., Straughan, B. P. & Treverton, J. A. XPS studies of zirconium complexes on polymer surfaces. *Appl. Surf. Sci.* **68**, 243–250 (1993).
53. Pettersson, L. A. A., Lucimara, S. R. & Inganas, O. Modeling photocurrent action spectra of photovoltaic devices based on organic thin films. *J. Appl. Phys.* **86**, 487–496 (1999).
54. Li, G. *et al.* High-efficiency solution processable polymer photovoltaic cells by self-organization of polymer blends. *Nat. Mater.* **4**, 864–868 (2005).

## Acknowledgments

The work was supported by the NSFC (Nos. 21004019, 51173040, 91023039, 51303052, 91333204), the Ministry of Science and Technology of China (973 project, No. 2014CB643501 and 863 project, No. 2011AA050523), the Beijing NOVA Program (No. 2010B038), SRFDP (No.20100036120007), Program for New Century Excellent Talents in University (NCET-12-0848), the 111 Project (B12034), and Fundamental Research Funds for the Central Universities, China (11QG18, 13ZD11).

## Author contributions

Z.A.T., S.S.L., J.L. and Y.F.L. designed, fabricated and characterized the devices. D.P.Q. and J.H.H. synthesized the polymer PBDTBDD. Z.A.T. and F.Z.W. conducted the optical simulation. All authors discussed the results, and Z.A.T., S.S.L. and Y.F.L. write the manuscript.

## Additional information

**Supplementary information** accompanies this paper at <http://www.nature.com/scientificreports>

**Competing financial interests:** The authors declare no competing financial interests.

**How to cite this article:** Tan, Z. A. *et al.* High performance polymer solar cells with as-prepared zirconium acetylacetonate film as cathode buffer layer. *Sci. Rep.* **4**, 4691; DOI:10.1038/srep04691 (2014).



This work is licensed under a Creative Commons Attribution 3.0 Unported License. The images in this article are included in the article's Creative Commons license, unless indicated otherwise in the image credit; if the image is not included under the Creative Commons license, users will need to obtain permission from the license holder in order to reproduce the image. To view a copy of this license, visit <http://creativecommons.org/licenses/by/3.0/>